Journal Pre-proofs

Full Length Article

Modelling percentages of cohesive and adhesive debonding in bitumen-aggregate interfaces using molecular dynamics approaches

Pengxu Chen, Xue Luo, Yangming Gao, Yuqing Zhang

Please cite this article as: P. Chen, X. Luo, Y. Gao, Y. Zhang, Modelling percentages of cohesive and adhesive debonding in bitumen-aggregate interfaces using molecular dynamics approaches, *Applied Surface Science* (2021), doi: https://doi.org/10.1016/j.apsusc.2021.151318

This is a PDF file of an article that has undergone enhancements after acceptance, such as the addition of a cover page and metadata, and formatting for readability, but it is not yet the definitive version of record. This version will undergo additional copyediting, typesetting and review before it is published in its final form, but we are providing this version to give early visibility of the article. Please note that, during the production process, errors may be discovered which could affect the content, and all legal disclaimers that apply to the journal pertain.
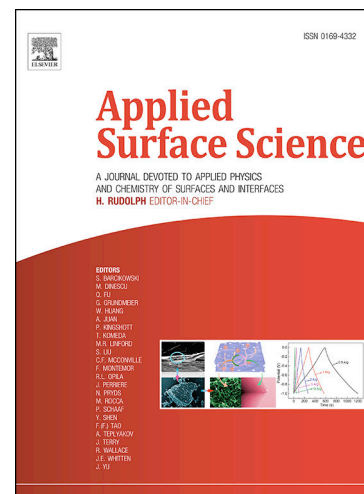
Modelling percentages of cohesive and adhesive debonding in bitumen-aggregate interfaces using molecular dynamics approaches

Pengxu Chen [a], Xue Luo [a], Yangming Gao [b], Yuqing Zhang [c,*]

[a] College of Civil Engineering and Architecture, Zhejiang University, 866 Yuhangtang Road, Hangzhou 310058, Zhejiang, China

[b] Section of Pavement Engineering, Faculty of Civil Engineering & Geosciences, Delft University of Technology, Stevinweg 1, 2628 CN, Delft, The Netherlands

[c] Department of Civil Engineering, Aston University, Aston Triangle, Birmingham B4 7ET, UK

Email: pengxuchen@zju.edu.cn (Pengxu Chen), xueluo@zju.edu.cn (Xue Luo), Y.Gao-3@tudelft.nl (Yangming Gao), y.zhang10@aston.ac.uk (Yuqing Zhang).

* Corresponding Author.

Address: Aston Triangle, Birmingham, B4 7ET, U.K.

Tel: +44 121-204-3391

Abstract

When an asphalt mixture cracks, adhesive debonding occurs along bitumen-mineral interfaces and cohesive debonding occurs within bitumen films. At microscale, the two debonding processes can happen simultaneously but it is unknown for their percentages. This study aims to determine the percentages for cohesive and adhesive debonding and investigate how the material and external factors can affect these percentages using molecular dynamics (MD) modelling. The pull-off simulations of bitumen-calcite interfaces were performed at different bitumen film thicknesses, pull-off velocities and temperatures. The percentages of cohesive debonding were calculated as the area ratio of the remained bitumen molecules over the total interface. Results show that the percentage of cohesive debonding increases from 29% to 65% with thicker bitumen films, and decreases from 86% to 59% with higher loading velocities. When temperature rises, the percentage of cohesive debonding increases from 61.3% to 88.2%. Quartz presents a weak adhesion to bitumen, and thus a complete (100%) adhesive debonding occurs regardless of bitumen thickness. Microcline shows a very strong adhesion to bitumen due to its high polarity. The modelled cohesive debonding percentage with different variables were verified and found consistent with the laboratory pull-off testing results available from the existing studies.

Key words

Bitumen-aggregate interface; Cohesive debonding; Adhesive debonding; Molecular dynamics; Pull-off simulation

1 Introduction

Cracking is one of the major distresses in asphalt pavements, which will directly threaten the safety and reduce the service life of the pavements [1]. Various research has been conducted to investigate the cracking in asphalt materials [2-6]. AASHTO defined three patterns of cracking in asphalt mixtures [7], including adhesive cracking, cohesive cracking and the mix of these two conditions. Adhesive cracking occurs at the interfaces between the bitumen and the aggregate surfaces, while cohesive cracking occurs within the coating film of the bitumen. The adhesive cracking and the cohesive cracking can happen simultaneously in the asphalt mixtures when subjected to the traffic or environmental loadings [8].

Cracking behaviors in asphalt mixtures ascribe to the failure and debonding between bitumen and aggregates at the microscale. Zhang et al. [9] found that the bond energy between bitumen and aggregates consists of both adhesive bond energy and cohesive bond energy and is formulated using the two bond energies by a certain ratio α:

$$\Delta G = \alpha \Delta G^c + (1-\alpha)\Delta G^a \tag{1}$$

where ΔG^c is the cohesive bond energy; ΔG^a is the adhesive bond energy; α is the percentage of the cohesive fracture.

They also proposed a compressive crack initiation criterion for any viscoelastic materials with pre-existing flaws or void, as defined in Eq. (2):

$$RPSE_c - \frac{1}{2}DPSE_c = \frac{7}{6}\pi\frac{\Delta G}{c} \tag{2}$$

where $RPSE_c$ and $DPSE_c$ are the recoverable pseudostrain energy and the dissipated pseudostrain energy at the critical moment when wing cracks are initiated; c is the critical crack size.

By simplifying the crack initiation criterion, a model was proposed to predict the compressive strength of the asphalt mixture considering the bond energy, critical crack size, and the elastic

modulus of the asphalt mixture:

$$\sigma_u = \sqrt{\frac{7}{2}\pi\frac{\Delta G \cdot E_R}{c}} \tag{3}$$

where E_R is the elastic modulus of asphalt mixture; c is the critical crack size.

From Eq. (1) above, it can be found that the percentage of cohesive/adhesive bonding (debonding) directly determines the total bond energy ΔG at the bitumen-aggregate interfaces. Eqs. (2) and (3) show that the total bond energy ΔG contributes largely to the crack initiation and the strength of asphalt mixtures.

The bond energy ΔG in bitumen-aggregate interfaces can be better understood by investigating the debonding mechanism at bitumen-aggregate interfaces. From an industrial perspective, this is critical to prevent cracks and improve the cracking resistance of asphalt mixtures. Additionally, the material (compressive or tensile) strength of the asphalt mixtures can be predicted, which is beneficial to improve the mechanical performance of asphalt mixtures during the design phase and potentially extend the service life of the pavements. However, without knowing the percentages of the cohesive bond energy, the total bond energy ΔG cannot be effectively obtained and thus the crack initiation [Eq. (2)] and the material strength [Eq. (3)] will not be accurately predicted. In addition, it has been confirmed from experiments and simulations that the adhesion bond energy in bitumen-aggregate interface is generally greater than the cohesive one [9, 37]. This indicates that the total bond energy of bitumen-aggregate interface would be greater provided that the adhesive bonds take up a larger proportion out of the total bond energy. This provides theoretical guidance for the debonding mechanism, which offers a direction for selecting and modifying the raw materials in pavement engineering.

A number of researchers have focused their studies either on the adhesion of bitumen-aggregate interface or the cohesion of bitumen. Five theories are commonly used to explain the adhesion behavior between bitumen and aggregate, including mechanical adhesion theory [10, 11], chemical reaction theory [12, 13], surface energy theory [14, 15], molecular orientation theory [16], electrostatic theory [17] and weak boundary theory [18, 19]. The cohesion is normally determined by the surface free energy of the bitumen, which can be obtained by nanoindentation test or contact angle test [14, 20]. More studies are focused on the utilization of additives to improve the cohesion

of the bitumen [21, 22], the use of anti-stripping agents to improve the interfacial adhesion between bitumen and aggregate [23, 24] and numerical modelling of cohesive and adhesive cracking in the asphalt mixtures [25, 26]. However, few studies have investigated the percentages of the adhesive debonding and the cohesive debonding that are occurring simultaneously during the crack process in the asphalt mixture.

To observe and measure the cohesive and adhesive debonding from the macroscopic experimental perspective, pneumatic adhesion pull-off strength testing instrument (PATTI) is mostly adopted to study the strength and debonding patterns during pull-off debonding between bitumen and aggregate [27]. Zhang et al [28] investigated the effects of bitumen hardness, temperature and bitumen film thickness on the debonding patterns between the bitumen and the aggregates based on the PATTI test and peel test. It was found that the bond energy of the harder bitumen was greater than that of the softer bitumen when subject to cohesive damage. When temperature decreased, the cohesive debonding becomes gradually less and a mix of adhesion/cohesive debonding has appeared. Cohesive debonding occurred when the bitumen thickness increased from 0.2 mm to 0.9 mm. Moraes et al [29] proposed a bitumen bond strength (BBS) test based on PATTI to investigate the bond energy of the bitumen-aggregate interface in the presence of water. Results showed that the BBS test can successfully evaluate the effect of water conditioning time on the bitumen's bonding strength with the aggregate. In the absence of water, the debonding usually occurs within the bitumen (cohesive damage). In the presence of water, the failure converts to adhesive debonding gradually. In contrast, the BBS test conducted by Chaturabong et al [30] showed that the damage in the asphalt mastics was still cohesive debonding even after 96 h of wet conditioning, which indicates that the moisture damage of the asphalt mixture is more related to cohesive damage. Canestrari et al [31] used a modified PATTI test to study the effect of water on the cohesion and adhesion of the bitumen-aggregate interface. It was found that the modified PATTI under dry conditions can characterize the cohesion of the bitumen, and the influence of water on the adhesion is greater than the cohesion. Test results showed that porphyry aggregates exhibit cohesive debonding under all conditions, while limestone aggregates cause both cohesive and adhesive debonding. Yuan et al [32] investigated the bond energy between the bitumen and the aggregates at different aging stages using the BBS and AFM tests. It was found that the bond strength was influenced by the cohesive and adhesive forces. With an increasing aging, the

cohesive bond energy within the bitumen increases, while the adhesive bond energy strengthens initially and then decreases, which demonstrates that moderate aging benefits bond strength whereas severe aging does not.

The above studies have investigated the cohesive and adhesive debonding in the asphalt mixtures through experimental tests (mainly by pull-off tests) and resulted in the preliminary understanding to the cohesion and adhesion in the materials at the macroscale dimensions. Nevertheless, further studies from nanoscale dimension are needed to reveal the fundamental mechanisms of the effects of the material, loading and environmental factors on the cohesive and adhesive debonding in the bitumen-aggregate interface systems. Accordingly, at macro level, the bond strength between bitumen and aggregates as well as the strength of asphalt mixtures can be further evaluated and potentially predicted.

As an emerging technique for material modelling, molecular dynamics (MD) is currently widely used in all types of materials including the pavement construction materials [33, 34]. By building molecular/atomic models of bitumen and aggregate, MD can simulate the motion and interaction behavior of the molecules and atoms in the force field to investigate the mechanism of material properties at the nanoscale. Much of the current MD research on bitumen pays particular attention to the physical properties of the materials, including density, glass transition, solubility, cohesion as well as the adhesion properties of the bitumen-aggregate interface. Zhang and Greenfield [35, 36] originally developed MD models for the bituminous materials. Xu et al. has conducted numerous studies on bitumen and bitumen-aggregate interfacial properties using the MD, including the cohesion within the bitumen film and the interfacial adhesion between the bitumen and minerals [37], thermodynamic properties and self-healing ability of aged bitumen [38], properties of reclaimed asphalt pavement binder with rejuvenator [39], and tensile simulation of the bitumen-aggregate interface [40]. Gao et al. [41, 42] used MD to compare the adhesion between different minerals and bitumen in consideration of the aging and moisture conditions of the bitumen, which provides a theoretical support to elucidate the adhesion mechanism between the bitumen and the aggregates from the nanoscale. Hou et al. [43] developed a molecular model of bitumen to study the cracks in bitumen. It was found that the natural distribution of atoms at the nanoscale affected the intrinsic defects of bitumen, which in turn affects the initiation and propagation of the cracks in bitumen. Lu and Wang [44, 45] used MD to apply tensile and shear forces at the bitumen-mineral

aggregate interface and investigated the failure behavior of the interface by different loading modes and mechanical analysis. Luo et al. [46, 47] used MD to study the mineral anisotropy effect on the adhesion behavior of the bitumen-mineral interface. In summary, unlike identifying the debonding behaviors at bitumen-aggregate interfaces from macroscopic view, MD plays a significant role in the understanding and modelling the debonding behavior of the bitumen and the bitumen-aggregate interfaces at atomic scale. However, none research has used the MD to evaluate and determine the percentages of the cohesive and adhesive damage in the debonding process for the bitumen-aggregate interface under a pull-off tensile load.

The objective of this study is to use the molecular dynamics approaches to investigate the debonding modes of bitumen-aggregate interfaces when subjected to a pull-off tensile load and determine the percentages of the cohesive and adhesive debonding. The flowchart of this research is shown in Fig. 1. First, a model of the bitumen-calcite interface was constructed. A dynamic equilibration and pull-off simulations of the interface were performed using an augmented consistent valence (cvff_aug) force field [48]. Then, the percentages of adhesive and cohesive debonding in the interface will be determined when different bitumen film thicknesses, pull-off loading velocities and temperatures were studied. The cohesive and adhesive debonding mechanisms will be investigated using interaction energy change during the pull-off process. Then, the cohesive and adhesive debonding will be modelled for the bitumen and different minerals including quartz and microcline. MD simulation results under different conditions were verified and validated by laboratory test or simulation results available from the literatures.
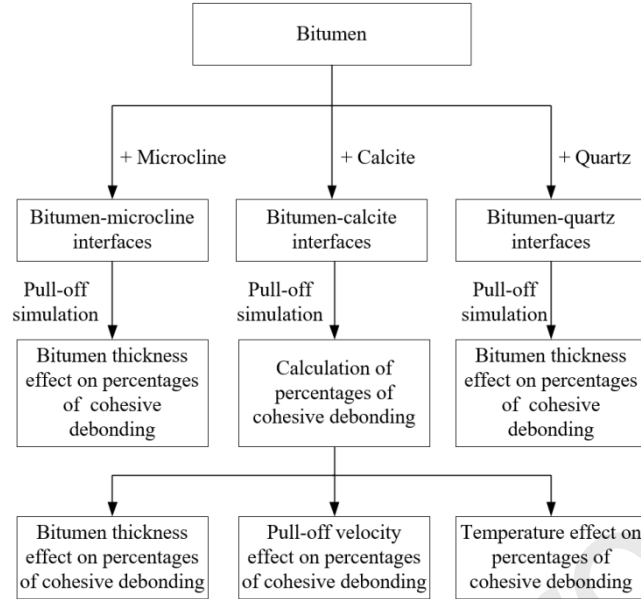
Fig. 1 Flowchart of this research

2 Molecular dynamic simulation models

2.1 Force field for bitumen-aggregate interface model

The energy of a molecular system is the sum of potential energy and kinetic energy. The potential energy of the molecules can usually be expressed as a function of position coordinates, which is called the potential function. The potential function of a complex molecular system is usually a combination of several potential energy types. The force field is a set of potential functions that define the interaction behavior between molecular atoms, including the form of the potential function and the potential energy parameters. The form of the potential function varies in different force fields. Therefore, it is crucial to find a suitable force field for the bitumen-mineral aggregate system for the sake of modelling accuracy. The cvff_aug, a force field applicable to both inorganic and organic materials, can simulate the material systems composed of polymers and minerals. This force field has been successfully implemented in the simulation of the bitumen-aggregate interface and is adopted in this study. The augmented consistent valence force field is defined as follows.

$$E_{cvff} = E_{valence} + E_{non-bond} \tag{4}$$

$$E_{valence} = E_{bond} + E_{angle} + E_{dihedral} + E_{improper} \tag{5}$$

$$E_{non-bond} = E_{van\,der\,Waals} + E_{Coulomb} \tag{6}$$

Eqs. (4)-(6) show that the potential function of the cvff_aug force field consists of the valence

bond potential ($E_{valence}$) and the non-bond potential ($E_{non-bond}$). More specifically, the valence

bond potential contains bond stretching term (E_{bond}), bond angle bending term (E_{angle}), dihedral

angle twisting term ($E_{dihedral}$) and improper angle bending term ($E_{improper}$); the non-bond potential

consists of van der Waals potential ($E_{van\,der\,Waals}$) and Coulomb potential ($E_{Coulomb}$). The details

of every potential functions are represented as follows.

$$E_{bond} = \sum_i K_b (l_i - l_i^0)^2 \tag{7}$$

Eq. (7) describes the potential function of the bond stretching term, which represents the

potential between atoms bonded in a molecule. The bond lengths between atoms are not constant,

but fluctuate slightly around their equilibrium lengths, so they are in the form of simple harmonic

vibrations. Where K_b represents the stiffness constant of the bond stretching, l_i and l_i^0

represent the bond length of the i-th bond and its equilibrium bond length, respectively.

$$E_{angle} = \sum_i K_\theta (\theta_i - \theta_i^0)^2 \tag{8}$$

Eq. (8) suggests the potential function of the bond angle bending term, whose general form is

also a simple harmonic vibration. Where K_θ represents the stiffness constant of the bond angle

bending, θ_i and θ_i^0 represent the angle of the i-th bond angle and its equilibrium bond angle,

respectively.

$$E_{dihedral} = \sum_i K_T [1 + d \cos n(\varphi_i - \varphi_i^0)] \tag{9}$$

The dihedral angle is formed by the four successive-bonded atoms in a molecule is unstable

and easily twisted. Eq. (9) reveals dihedral angle twisting potential function. Where K_T is the

stiffness constant of the dihedral torsion, φ_i and $\varphi_i^{\,0}$ are angle of the i-th dihedral angle and its

equilibrium dihedral angle, respectively, and d and n are integer parameterizations of the atomic

system.

$$E_{improper} = \sum_i K_\omega [1 - \cos 2\omega_i] \tag{10}$$

Eq. (10) represents the bending potential of the improper angle. Where, K_ω represents the

bending stiffness coefficient of the improper angle, and ω_i represents the improper angle of the

two planes formed by the first three atoms and the last three atoms of the four successive bonded atoms.

$$E_{van\,der\,Waals} = \sum_{i,j} 4\varepsilon \left[\left(\frac{\sigma_{ij}}{r_{ij}} \right)^{12} - \left(\frac{\sigma_{ij}}{r_{ij}} \right)^{6} \right] \qquad (11)$$

Van der Waals interaction is the top contributor to the pair potential in the non-bond potential. The target includes atoms separated by more than two bonds in one molecule or pair atoms belonging to different molecules. The form of van der Waals potential in the non-bond potential is shown in Eq. (11) which is called the Lennard-Jones (LJ) potential, or the 12-6 potential. Where $\sigma_{i,j}$ and ε are the two potential parameters defining the van der Waals interaction, and r_{ij} denotes the distance between atomic pairs.

$$E_{Coulomb} = \sum_{i,j} \frac{q_i q_j}{4\pi\varepsilon_0 r_{ij}} \qquad (12)$$

The ions or atoms in a force field are partially charged so there is electrostatic attractions or repulsions between these atoms in the form of Coulomb potential as shown in Eq. (12). Where q_i and q_j are the charges of the i-th and j-th ions or atoms, respectively, $4\pi\varepsilon_0$ is called the effective permittivity, and r_{ij} is the distance between ions or atoms.

2.2 Bitumen models

Bitumen is a highly complex polymer composed of hydrocarbons with different molecular weights [49]. Because of its complicated chemical components, it is difficult to model the composition of bitumen using one specific molecule representative. According to similar molecular characteristics and chemical properties, American Society of Testing Materials (ASTM) classifies the chemical composition of bitumen into four components (SARA), namely saturate, aromatic, resin and asphaltene [50]. The SARA contents vary in bitumen of different qualities. Currently, Li and Greenfield [51] have proposed 12-molecule models of representative bitumen AAA-1, AAD-1 and AAM-1 in SHRP program based on the four-fraction classification, in which each component consists of several organic molecules, and the combined 12 molecules represent the chemical components of the bitumen. These models have been proved reasonable and reliable in previous studies [38, 41, 42]. Thus, the 12-molecule model of the AAA-1 bitumen was selected as the

representative for the simulations in this study. The AAA-1 bitumen molecules and their proportions are shown in Table 1.

Table 1 Molecules and proportions in AAA-1 bitumen model

Fraction	Molecules	Molecular formula	Number of molecules	Mass fraction (%)
Saturate	Squalane	$C_{30}H_{62}$	8	5.4
	Hopane	$C_{29}H_{50}$	8	4.9
Aromatic	PHPN	$C_{35}H_{44}$	22	16.2
	DOCHN	$C_{30}H_{46}$	26	16.8
	Quinolinohopane	$C_{34}H_{47}N$	8	6.0
	Thioisorenieratane	$C_{40}H_{60}S$	8	7.3
Resin	Benzobisbenzothiophene	$C_{18}H_{10}S_2$	30	13.8
	Pyridinohopane	$C_{30}H_{45}N$	8	5.3
	Thrimethybenzeneoxane	$C_{29}H_{50}O$	10	6.6
	Asphaltene-phenol	$C_{42}H_{50}O$	6	5.5
Asphaltene	Asphaltene-pyrrole	$C_{66}H_{81}N$	4	5.6
	Asphaltene-thiophene	$C_{51}H_{62}S$	6	6.7

The AAA-1 bitumen model was built using the Amorphous Cell module in software Materials Studio 8.0 [52]. First, a cubic model was built by filling 12 molecules of the AAA-1 bitumen model with an initial density of 0.1 g/cm^3, and after energy minimization using geometric optimization, the bulk bitumen model was subjected to dynamic equilibration for 500 ps under NPT ensemble (constant molecules, constant pressure, and constant temperature) with temperature of 298 K and pressure of 0.1MPa. The Nose-Hoover-Langevin thermostat and Andersen barostat were used to ensure that the system was maintained near the target temperature and pressure. In the simulation, the time step was set to 1 fs. After dynamics equilibration, the volume of the bitumen model was shrunk and the density was finally stabilized at 0.95 g/cm^3. This density was used as the target density to build the bitumen confined layer model. The bitumen confined layer model is non-periodic in the [0 0 1] direction, so the bitumen model has a flat surface in the z-direction, which is used to build the next bitumen-aggregate interface model. Larger simulation scale results in less effect of different bitumen conformations and promises a more stable system, so the dimensions of the established bitumen confined layer model in the [1 0 0], [0 1 0] and [0 0 1] directions are set respectively 59.0 Å, 59.0 Å and 30.1 Å.

2.3 Mineral aggregate models

Different aggregate minerals have distinct chemical composition, and thus present different adhesive abilities with bitumen due to varying degrees of non-bond interactions [41]. In this study, three minerals, including a weakly alkaline mineral (calcite), a strongly alkaline mineral (microcline) and an acidic mineral (quartz), were adopted in this study to model the bitumen-aggregate interfaces. Among them, the bitumen-calcite aggregate interfaces are studied comprehensively to investigate the debonding modes under different conditions while the interfaces modelled by microcline and quartz are studied only at different bitumen thicknesses. These interfacial models are finally compared to investigate the effect of mineral types on interfacial debonding behaviors.

The results of the mineral liberation analyzer (MLA) test conducted by Zhang et al. [53] showed that in limestone, more than 90% of the minerals are calcite. Therefore, for the aggregate model, the calcite model was used to represent the limestone aggregates for simulating bitumen-aggregate interfacial debonding behavior. First, the crystal structure of calcite was export from the Cambridge Structural Database (CSD). Its unit cell structure and lattice parameters are shown in Table 2. The previous study [47] showed that due to the anisotropy of the mineral structure, when the unit cell of calcite is cleaved along the [0 1 8] direction, the adhesion strength of the exposed surface to the bitumen is the strongest. In this study, the mineral was cleaved along this direction with a thickness of 15.3 Å. In order to be attached to the bitumen confined layer, this surface needs to be re-cleaved as a rectangular surface. The cleaved surface was repeated in the U and V directions using the Supercell module to model the mineral aggregate so that the final dimensions in the U and V directions were up to 64.9 Å and 64.3 Å.

The modeling process of quartz aggregate is as follows: first, the structure of quartz crystal was derived from the CSD, as shown in Table 2. The unit cell was cleaved along the [1 0 1] direction to expose the surface with a thickness of 16.7 Å. In order to attach to the bitumen confined layer, this surface was recleaved to a rectangular surface. The cleaved surface was repeated along the U and V directions using the Supercell module to model the mineral aggregate, with the final dimensions up to 65.7 Å and 63.8 Å in the U and V directions. Modelling of the microcline mineral aggregate is similar to that of the quartz mineral aggregate model, except that the cleaving direction when constructing the surface was [1 0 0] and the thickness was 15.4 Å, and the final size of the microcline aggregate model is 64.8 Å × 65.0 Å.

Table 2 Unit cell of minerals and lattice parameters

Minerals	Chemical formula	Unit cell structure	Lattice parameters
Calcite	$CaCO_3$		a=b=4.990 Å, c=17.061 Å; $\alpha = \beta$ =90°, γ =120°
Quartz	SiO_2		a=b=4.910 Å, c=5.402 Å; $\alpha = \beta$ =90°, γ =120°
Microcline	$KAlSi_3O_8$		a =8.573 Å, b= 12.962 Å, c=7.219 Å; α =90.6°, β =115.9°, γ =878°
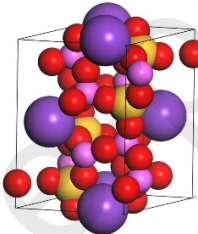
2.4 Bitumen-calcite aggregate interfacial model

To achieve large-scale and more accurate MD simulations, the bitumen-aggregate interface model will adopt periodic boundary conditions (PBC) to achieve model repetition in x, y, and z dimensions. First, the bitumen confined layer model is added to the top of the rigid calcite aggregate model (with surface cleaved along [0 1 8]) using the Build Layers module. To eliminate the effect of periodic boundaries on the adhesion during dynamic equilibration, a vacuum slab with a thickness of 50 Å was added above the bitumen. The constructed bitumen-calcite aggregate interface model whose geometry is 61.9 Å × 61.6 Å × 118.6 Å is shown in Fig. 2. The interfacial model of bitumen-quartz aggregate and bitumen-microcline aggregate are constructed by the same means. The final dimensions of the bitumen-quartz aggregate model are 62.3 Å × 61.4 Å × 118.6 Å, and the dimensions of the bitumen-microcline aggregate model is 61.9 Å × 62.0 Å × 117.3 Å.
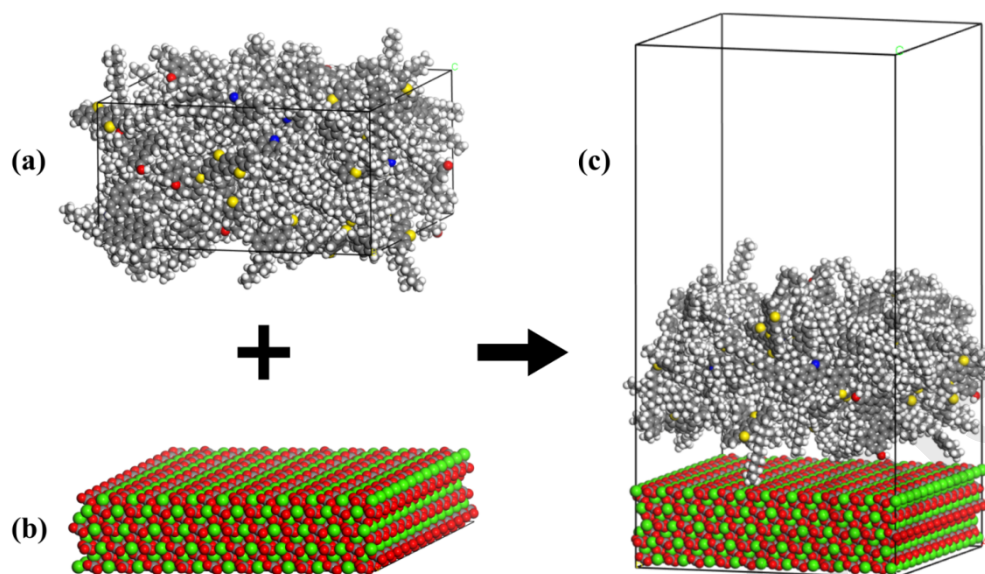
Fig.2 bitumen-calcite interfacial model: (a) AAA-1 bitumen confined layer model; (b) calcite mineral model; (c) bitumen-calcite aggregate interfacial model

3 Pull-off simulation of bitumen-calcite aggregate interface

3.1 Dynamic equilibration of bitumen-calcite aggregate interface

The established bitumen-calcite aggregate interface model underwent a dynamic equilibration using the open-source software LAMMPS (Large-scale Atomic/Molecular Massively Parallel Simulator) [54]. Firstly, the established bitumen-aggregate interface model system was energy minimized using the Polak-Ribiere version of the conjugate gradient (CG) algorithm, and then the dynamic equilibration of the system is performed. To ensure a constant rate of interfacial separation during the debonding simulation, the upper bitumen molecules were relaxed in the NVT ensemble (constant molecules, constant volume, and constant temperature), while the lower calcite aggregate atoms were fixed and remaining stationary as a rigid aggregate model in the NVE ensemble (constant molecules, constant volume, and constant energy). 12 Å of the cutoff distance was used in the simulation and the equilibration temperature is 298 K. The total simulation time was set to 1ns with a time step of 1fs, and the total energy of the system converged after 500 ps. Fig. 3(a) shows a schematic diagram of the interface model after the equilibration, from which it can be observed that the bitumen molecules adhere uniformly to the calcite mineral surface. The model was used for the following interface pull-off simulation.

3.2 Pull-off simulations at different conditions

To model the debonding of the bitumen molecules from the mineral surface, the calcite mineral substrate was fixed at the bottom and the top bitumen molecules (dark gray part in Fig. 3(a)(b)) were fixed as a bulk group which is moved along the z-direction at a specific velocity. The relative displacement remains unchanged for the bitumen molecules in this top fixed bulk part. Note that the thickness of the fixed part should be greater than the cutoff distance (12Å) to ensure the complete interaction between fixed and movable bitumen molecules.

Different factors are considered to investigate their effects on the debonding behaviors for the bitumen-aggregate interfaces. As shown in Table 3, five bitumen film thicknesses for every bitumen-mineral model, five loading rates and six temperatures are studied and their simulation details are displayed herein. Because the total bitumen thicknesses of bitumen-quartz and bitumen-microcline models after dynamic equilibration is smaller than the bitumen-calcite model, the bitumen film thicknesses for bitumen-quartz and bitumen-microcline models are thinner than bitumen-calcite model. Note that for different temperature groups, another 1ns dynamic equilibration at the corresponding temperature were performed to achieve the corresponding asphalt density. All the pull-off simulations are performed with PBC in x and y dimensions and non-PBC in z dimension. This means that the interfacial model was finite in z dimension and there was no periodic mineral above the bitumen molecules. The pull-off was performed under NVT ensemble. The fixed bitumen molecules were set at a constant velocity in the z-direction to simulate the debonding behavior of the bitumen-aggregate interface when subjected to tensile forces. The total displacement of more than 40 Å in the z-direction was run at a time step of 1 fs.

Table 3 Influence factors modelled in pull-off simulations

Influence factors	Values Selected					
Bitumen film thickness[1] (Å)	15.0	17.5	20.0	22.5	25.0	-
Loading rate[2] (Å/fs)	5×10^{-5}	7.5×10^{-5}	1×10^{-4}	1.25×10^{-4}	1.5×10^{-4}	-
Temperature[3] (K)	238	258	278	298	318	338
Mineral type[4]	Quartz	Microcline	-	-	-	-

[1] conducted under a pull-off velocity of 1×10^{-4}Å/fs and temperature of 298K.

[2] conducted under a bitumen film thickness of 25 Å and temperature of 298K.

[3] conducted under a bitumen film thickness of 25 Å and a pull-off velocity of 1×10^{-4}Å/fs.

[4] conducted under a pull-off velocity of 1×10^{-4}Å/fs and temperature of 298K with a bitumen film thickness of 10 Å, 12.5 Å, 15 Å, 17.5 Å and 20 Å respectively.

The trajectory file of the pull-off process and the interaction energy of all cases are output. The interaction potential energy is defined as follows,

$$E_{interaction} = E_{asphalt} + E_{aggregate} - E_{total} \tag{13}$$

where $E_{asphalt}$ is the potential energy of all bitumen molecules, $E_{aggregate}$ is the potential energy of calcite aggregate, and E_{total} is the total potential energy of the bitumen-aggregate interface system.

3.3 Calculation of the percentage of cohesive debonding

The MD output trajectory file was examined to investigate the interfacial debonding behavior using the post-processing software OVITO [55]. Firstly, the trajectory was positioned to the frame at the displacement of 40 Å in the pull-off simulation, as shown in Fig. 3(b), and it can be found that some bitumen molecules remained on the surface of the mineral aggregate after the pulling. The bitumen molecules remaining on the calcite surface were sliced off completely by adjusting the slicing slab width, as shown in Fig. 3(b)(c). The image of the sliced bitumen molecules in top view was binarized in black and white, where the black part is the residual bitumen molecules, as shown in Fig. 3(d). This figure can be used to define the percentage of cohesive debonding which is the ratio of the black area over the total cross-sectional area, since the black area represents the bitumen molecules that remained on the mineral surfaces and the separation occurred within the bitumen film. A pixel count was performed to calculate the percentage of black color (i.e., bitumen molecules) over the total area of all molecular profiles, and this percentage was recorded as the percentage of cohesive debonding. The white area in Fig. 3(d) represents the bitumen molecules detached from the surface and the separation occurred at the bitumen-aggregate interfaces, which defines the percentages of the adhesive debonding. The sum of the percentages for cohesive and adhesive debonding equals 100%.
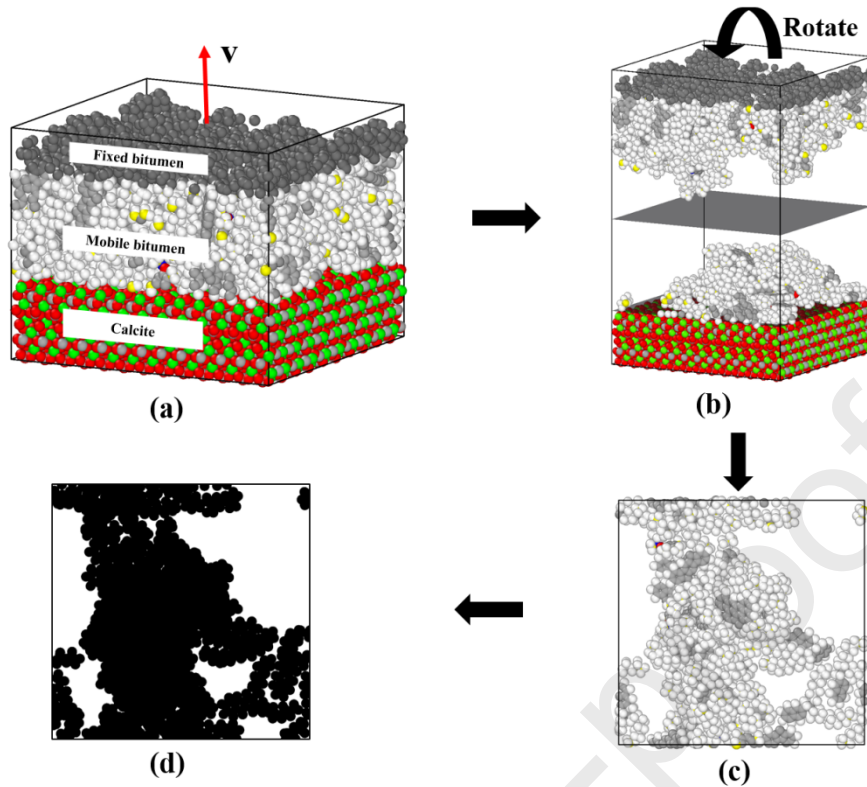
Fig. 3 Pull-off simulation (25Å, 1×10^{-4} Å/fs, 298K) and calculation of cohesive debonding percentage (a) bitumen-aggregate interfacial model after equilibration; (b) bitumen-aggregate interface after pull-off simulation (the slicing slab is shadowed); (c) top view of the residual bitumen molecules on the aggregate surface; (d) binarized top view of the residual bitumen on the aggregate surface (note, the ratio of black area over the total area in (d) representing the percentage of cohesive debonding during the pull-off simulations).

4 Effects of bitumen film thickness on interfacial debonding behavior

4.1 Percentage of cohesive debonding at different bitumen thicknesses

Bitumen thicknesses of 15 Å, 17.5 Å, 20 Å, 22.5 Å and 25 Å are investigated respectively. Fig. 4 shows three-dimensional MD models of the bitumen-calcite interfaces after pull-off simulations and Fig. 5 illustrates the binarized top views of the residual bitumen molecules on the calcite surface at different bitumen film thicknesses. The ratio of the black area to the total cross-sectional area was defined as the percentage of the cohesive debonding in this pull-off simulations.
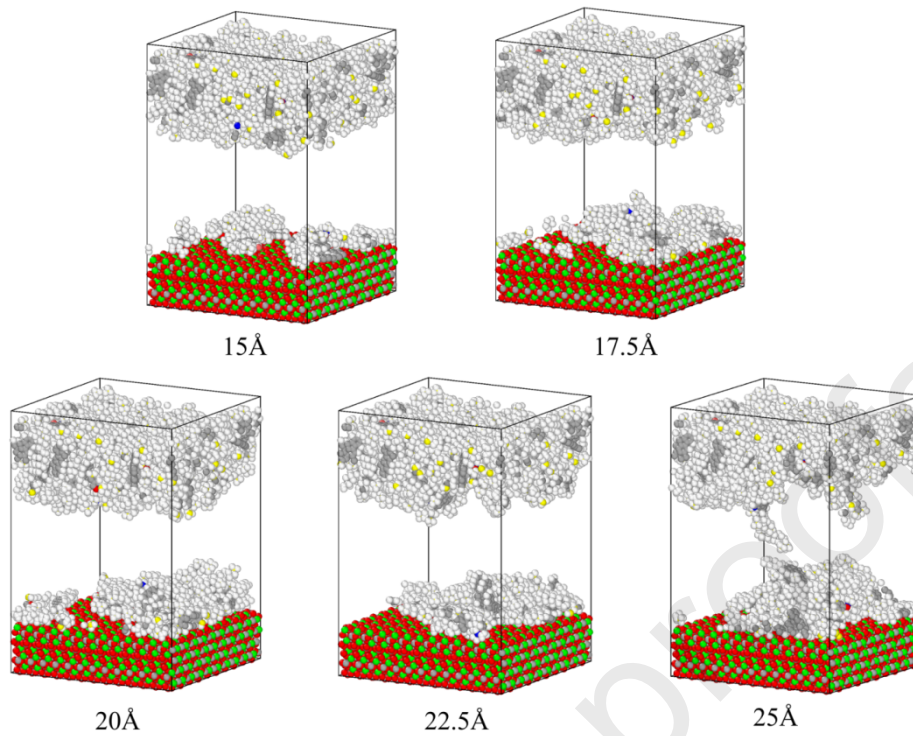
Fig. 4 Stereograms of the interfaces after pull-off simulations at different bitumen thicknesses
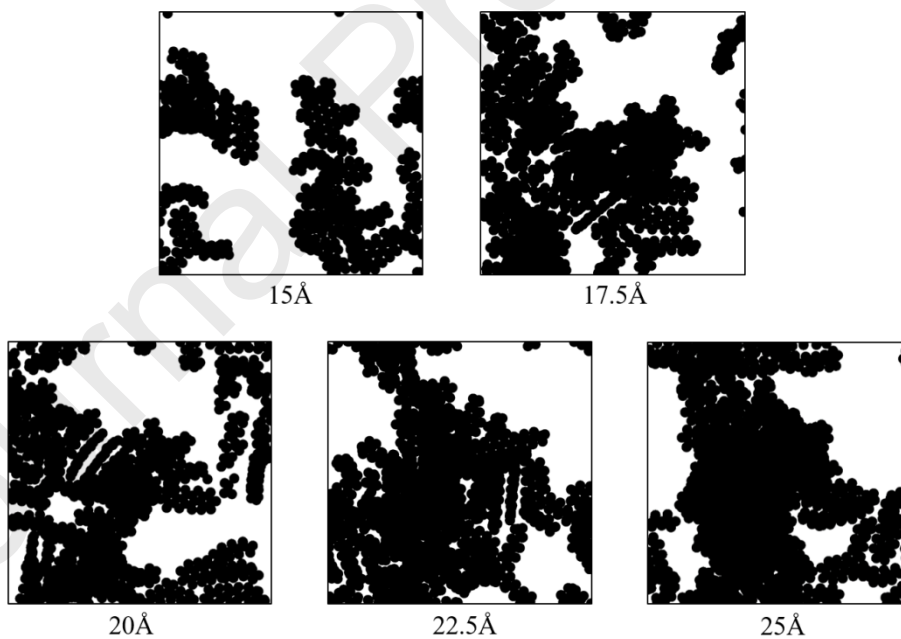
Fig. 5 Biniarized top view of residual bitumen molecules at different bitumen thicknesses

Fig. 4 shows that the bitumen-calcite interface models with different bitumen thicknesses were completely de-bonded after a pull-off displacement of 40 Å. As the bitumen thickness increases, the area of the residual bitumen molecules attached on the mineral surface increases. Based on Fig. 5, the percentages of cohesive debonding were calculated for different bitumen thickness and shown

in Fig. 6.
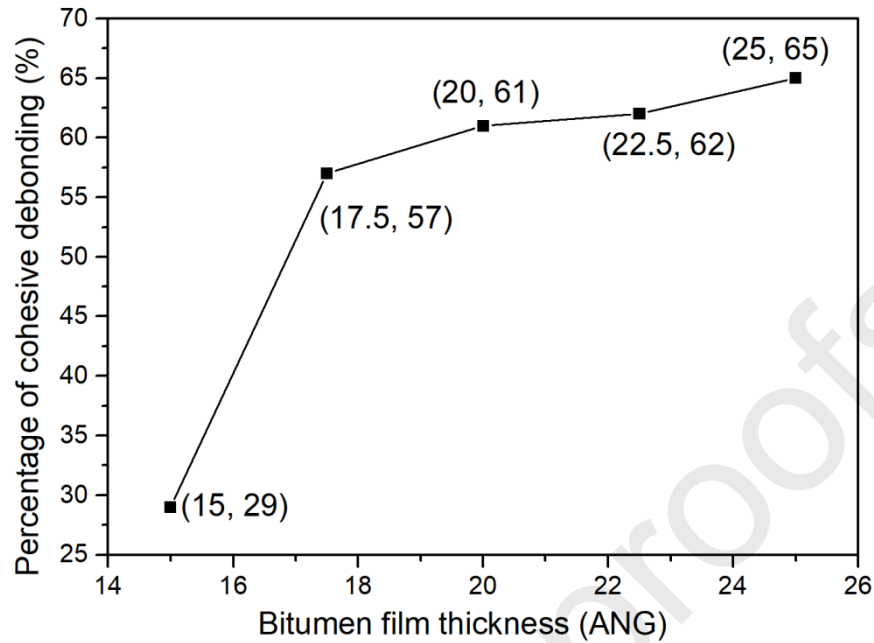
Fig. 6 Percentages of cohesive debonding at different bitumen film thicknesses

Fig. 6 demonstrates that as the bitumen film thickness increases from 15 Å to 25 Å, the percent of the cohesive debonding rises from 29% to 65%. It can also be found that the increase of the cohesive debonding percentage is exceedingly significant when the bitumen film thickness changes from 15 Å to 17.5 Å, rising from 29% to 57%. However, when the bitumen film thickness is greater than 17.5 Å, the increasing rate of the cohesive debonding percentage is moderate. This indicates that the cohesive debonding percentage is thickness sensitive when the bitumen film is thin. The results also show that when the bitumen film reaches a certain thickness, the cohesive debonding percentage exceeds the adhesive debonding percentage in the pull-off process of the bitumen-aggregate interface and the cohesive debonding becomes the dominating debonding mode. This coincides with the conclusion obtained in an existing study [56] that the cohesive debonding of the bitumen-aggregate interface becomes dominating as the bitumen thickness increases.

4.2 Interaction energy at different bitumen thicknesses

Fig. 7 shows the interaction energy curves of the pull-off debonding processes for the five different bitumen film thickness conditions. It can be found that the interaction energies between the bitumen and the aggregate for all thicknesses decline before recovering as the pull-off displacement increases. The interaction energy curves are consistent with the LJ potential energy curve. When the pull-off displacement of the bitumen molecules is small, there is a repulsive force

between the bitumen and the aggregate, and the interaction potential energies decline with the increase of the displacement. When the displacement attains the equilibrium position of the interaction force between the bitumen and the aggregate, the attractive force between bitumen and aggregate dominates the interaction potential which rises with the displacement. When the fixed bitumen together with the attracted movable bitumen molecules have moved and exceeded the cutoff distance from the aggregate surfaces, the interaction energy becomes stabilized and only represents the adhesion between the residual bitumen molecules and the calcite aggregate. Thus the higher the stabilized interaction energy, the more residual bitumen molecules remained on the aggregate surfaces and the higher percentage the cohesive debonding.
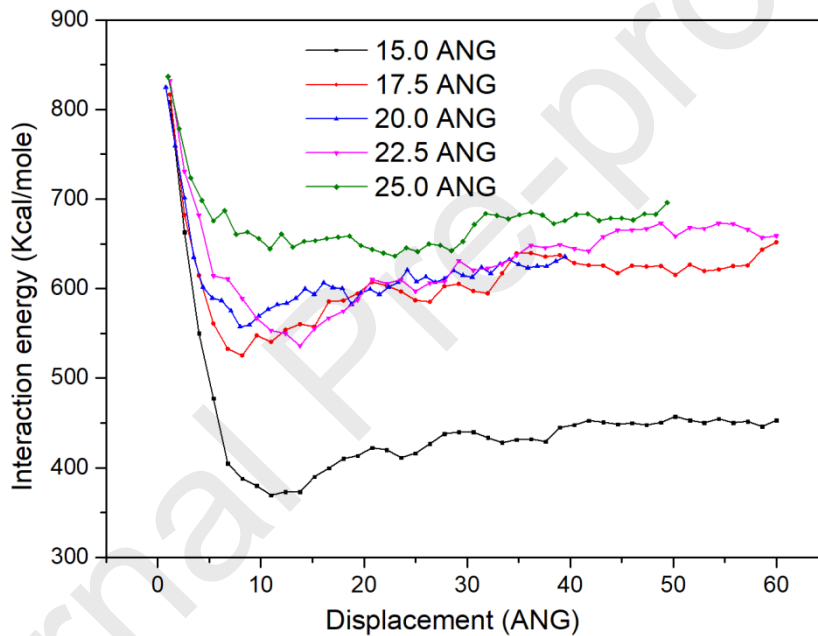
Fig. 7 Interface energy between the bitumen and the calcite aggregate at different bitumen

thicknesses

When the bitumen film is 15 Å, the stabilized interaction energy is low and stays around 450 Kcal/mole. This magnitude is in accord with the work of adhesion for bitumen-calcite interface from a previous research [37]. When the film thickness increases to 17.5 Å, the stabilized interaction energy increases significantly to more than 600 Kcal/mole, which is consistent with the change of the percentage of cohesive debonding. In the meantime, though the stabilized interaction energy gradually increases at the thickness higher than 17.5 Å, the increasing trend is not obvious, which also conforms to the change of the cohesive debonding percentage at thicknesses greater than 17.5

Å.

The fundamental mechanism for that thicker bitumen film thickness leads to more cohesive debonding is that a weak boundary layer exists next to the interface. As shown in Fig. 8, the bitumen molecules present three different bonding conditions to the mineral surface: (1) the molecules on the interface are double-linked to mineral surface at active sites (the "double-linked" group), having the strongest interface bond; (2) the molecules near the interface interacts with mineral surface by only one end of the molecular chain (the "one end-linked" group), leading to an intermediate interface bond; (3) the molecules away from the interface have no contact with mineral surface (the no-contact group), resulting in the weakest interface bond [57]. Hence, for a thin bitumen film, most bitumen molecules belong to the "double-linked" group and when pulled off, the adhesive debonding occurs. As the bitumen film becomes thicker, the "double-linked" bitumen molecules remains on the surface due to a strong interface bond and the "one end-linked" group are pulled off, leading to a higher percentage of cohesive debonding. As the bitumen film becomes much thicker, the pull-off de-bonding only happens within the weakest no-contact bitumen group with is away from the interface, leading to the highest percentage of cohesive debonding. This no-contact group has the weakest cohesion, so it is regarded as the weak boundary layer.
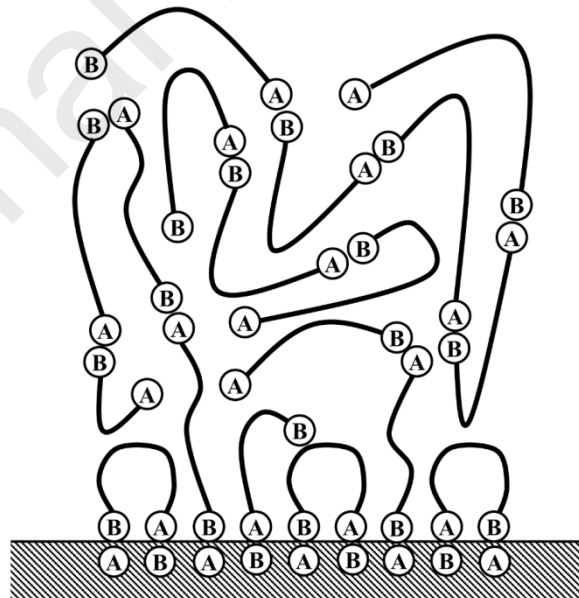
Fig.8 Distribution of bitumen molecules on mineral aggregate surface. (A and B both represent active sites and act as donor and acceptor respectively.)

4.3 Verification from laboratory pull-off tests on bitumen film thickness effect

Results from tests and other simulations in references are taken herein to evaluate the simulation results in this research. Note that the general trends of debonding behaviors in this simulation are comparable with that of laboratory testing results, even if the cleavage plane in mineral model do not coincide with the mineral surfaces in the experiments. Howson [58] conducted pull-off tests on a bitumen-substrate interface at different bitumen thicknesses. Table 4 presents the grey level of the sample holder substrate after pull-off tests. Grey level is calculated from the processed image of the failed interface of the bitumen-substrate, and it indicates the exposure of the substrate. The higher grey level is, the more adhesive debonding and the less cohesive debonding occur. From Table 4, it is found that the grey levels of both bitumen groups presented an overall decline when the bitumen film thickness increased from 5 μm to 40 μm, which Bitumen-AAB decreases from 0.76 to 0.02 and Bitumen-AAD decreases from 0.23 to 0.00. This means that more cohesive debonding and less adhesive debonding occur in thicker films. This trend is consistent with the simulated results, which the percentage of cohesive debonding increases with bitumen film thickness.

Table 4 Grey level[5] of the debonding interface at different thicknesses of bitumen films

Thickness (microns)	Bitumen-AAB	Bitumen-AAD
5	0.76	0.23
10	0.84	0.35
15	0.39	0.26
20	0.25	0.31
30	0.02	0.00
40	0.02	0.00

[5] refers to the exposed surface of the substrate after pull-off tests. Higher grey level means more adhesive failure and less cohesive failure.

5 Effects of pull-off velocity on interfacial debonding behavior

5.1 Percentage of cohesive debonding at different pull-off velocities

Pull-off velocities of 5×10^{-5}Å/fs, 7.5×10^{-5}Å/fs, 1×10^{-4}Å/fs, 1.25×10^{-4}Å/fs and 1.5×10^{-4}Å/fs are

investigated respectively. Fig.9 and Fig.10 show the three-dimensional MD models of the bitumen-aggregate interface after debonding at different velocities and the profiles of the residual bitumen after binarization.

$5 \times 10^{-5} Å/fs$ 　　　　　　　$7.5 \times 10^{-5} Å/fs$

$1 \times 10^{-4} Å/fs$ 　　　$1.25 \times 10^{-4} Å/fs$ 　　　$1.5 \times 10^{-4} Å/fs$
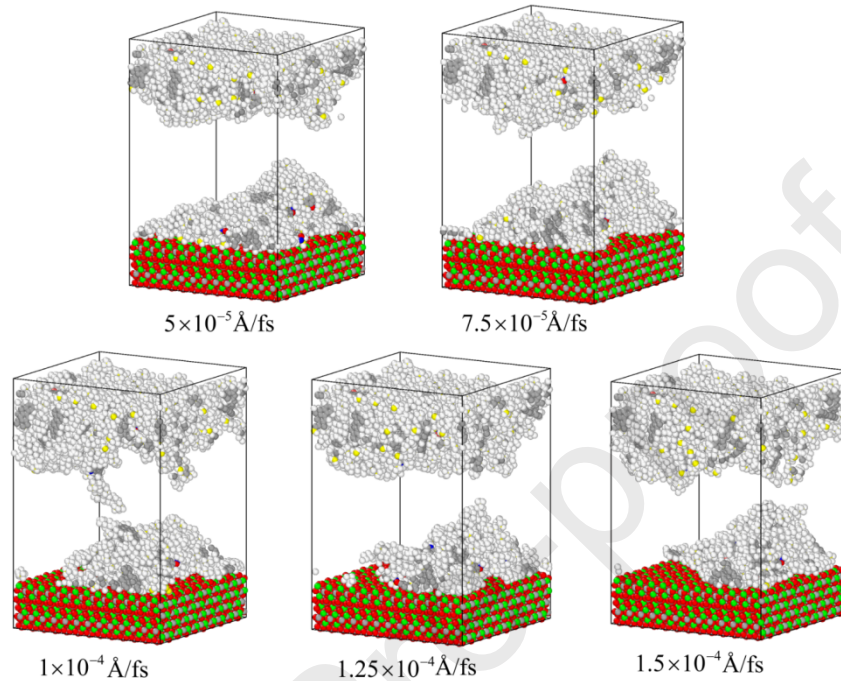
Fig. 9 Stereograms of the interfaces after pull-off simulation at different pull-off velocities

$5 \times 10^{-5} Å/fs$ 　　　　　　　$7.5 \times 10^{-5} Å/fs$

$1 \times 10^{-4} Å/fs$ 　　　$1.25 \times 10^{-4} Å/fs$ 　　　$1.5 \times 10^{-4} Å/fs$
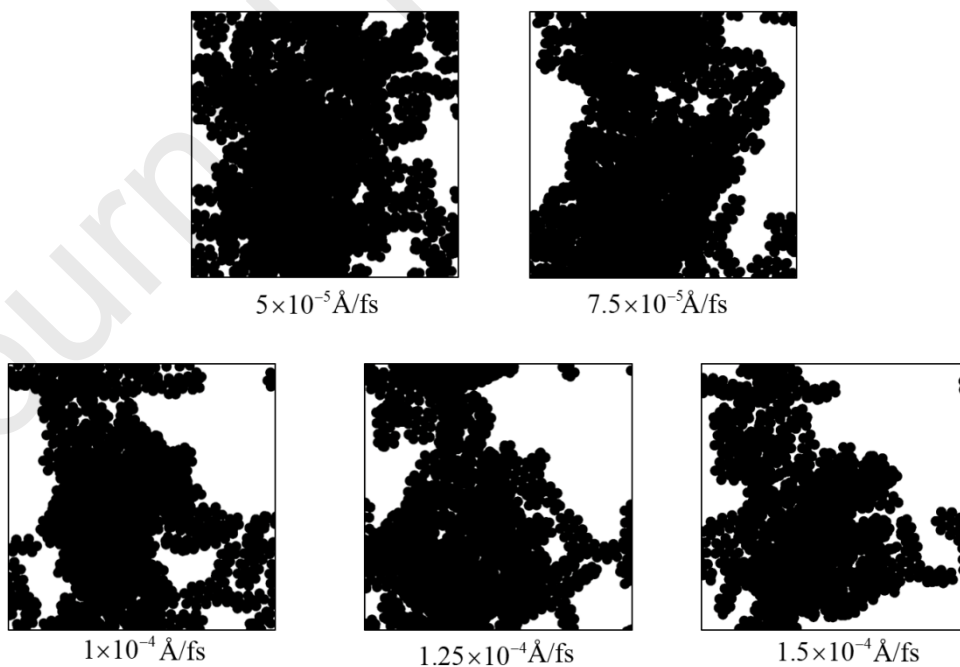
Fig. 10 Biniarized top view of residual bitumen molecules at different pull-off velocities

It can be seen from Fig. 9 that after a pull-off displacement of 40Å, the interfaces were

completely debonded for all velocities eventually, i.e., a complete separation of the upper mobile bitumen from the aggregate. The covered area by the bitumen molecules remaining on the calcite surface steadily shrinks with the increase of the pull-off velocity. The percentage of the cohesive debonding was calculated at different velocities, as shown in Fig. 11.
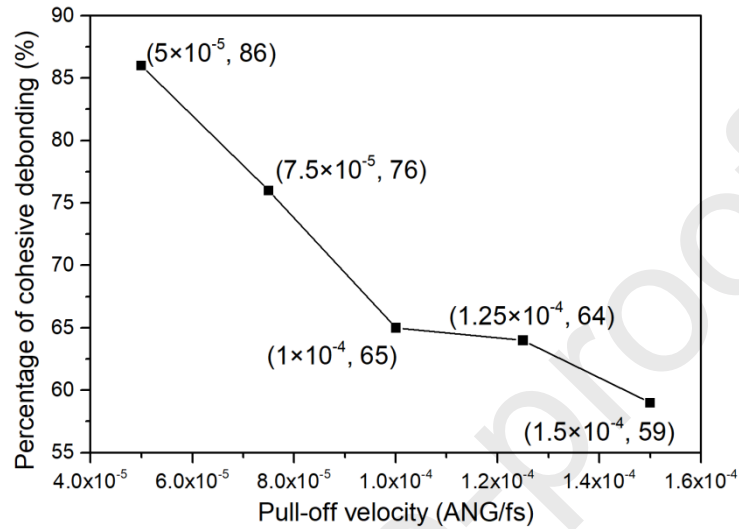
Fig. 11 Percentages of cohesive debonding at different pull-off velocities

As shown in Fig. 11, the percentage of cohesive debonding gradually decreases as the pull-off velocities increase, which is consistent with the findings on the relationship between the pull-off velocity and the amount of residual bitumen from the literature [40]. In particular, the percentage of cohesive debonding decreased linearly from 86% at 5×10^{-5} Å/fs to 65% at 1×10^{-4} Å/fs and slows down when the pull-off velocity is greater than 1×10^{-4} Å/fs. The percentage of cohesive debonding finally decreases to 59% when the pull-off velocity is increased to 1.5×10^{-4} Å/fs.

5.2 Interaction energy at different pull-off velocities

Fig. 12 reveals the changes of the interaction energy at different pull-off velocities. The stabilized interaction energy after pull-off simulation becomes smaller with a faster pull-off velocity, which indicates that the adhesion strength between the residual bitumen and the aggregate decreases, and more adhesive debonding occurs at the bitumen-aggregate interface. Moreover, compared to the increase in interaction energy after debonding from 1×10^{-4} Å/fs to 1.5×10^{-4} Å/fs, the change in interaction energy is greater when the pull-off velocity is increased from 5×10^{-5} Å/fs to 1×10^{-4} Å/fs, which confirms the different trends of the percentage of cohesive debonding in different velocity ranges in Fig. 11.
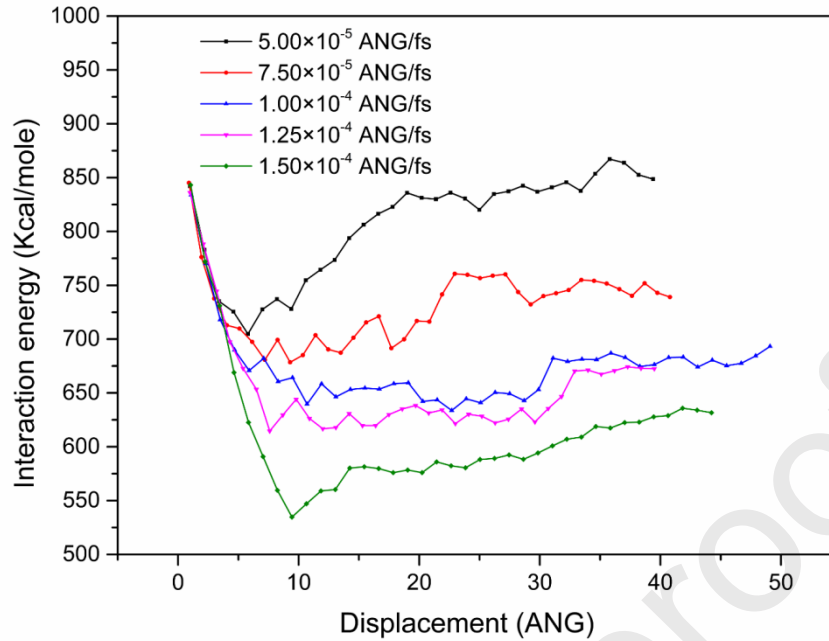
Fig. 12 Interface energy between the bitumen and the calcite aggregate at different pull-off velocities

The possible reason for this is that when the pull-off velocity is low, the mobile bitumen molecules move and easily return to equilibrium. However, as the pull-off velocity increases, the bitumen molecules are stretched in a short time, and the bitumen molecules act as springs. This makes the bitumen system an elastic molecular network, which leads to the mobile bitumen molecules clinging to the fixed bitumen are pulled off the aggregate surface [59].

5.3 Verification from extended finite element method on loading rate effect

Wang et al. [26] used stiffness degradation variable (SDEG) value to evaluate the adhesive and cohesive failure in an asphalt mixture based on an extended finite element method. The SDEG represents the adhesive failure of cohesive elements at the interface with a scale of 0-1. A larger SDEG values means more adhesive failure occurs. As can been seen from Table 5, the mean SDEG values presents an increase with a higher loading rate. It increases from 0.414 to 0.573 when loading rate rises from 0.5 mm/min to 5 mm/s. This indicates that more adhesive failure and less cohesive failure occur at the bitumen-aggregate interface at higher pull-off velocities, which is in agreement with the simulation results.

Table 5 The average values of stiffness degradation variable (SDEG) at different loading rates

Loading rate	Mean SDEG values
0.5 mm/min	0.414
0.5 mm/s	0.534
5 mm/s	0.573

6 Effects of temperature on interfacial debonding behavior

6.1 Percentage of cohesive debonding at different temperatures

Temperatures of 238K (-35 °C), 258K (-15 °C), 278K (5 °C), 298K (25 °C), 318K (45 °C) and 338K (65 °C) are adopted respectively when simulating the bitumen-aggregate interfacial debonding behavior. Fig. 13 and 14 show the three-dimensional interfacial models after pull-off simulations at different temperatures and the binarized profiles of residual bitumen, respectively.

238K (-35 °C)   258K (-15 °C)   278K (5 °C)

298K (25 °C)   318K (45°C)   338K (65 °C)
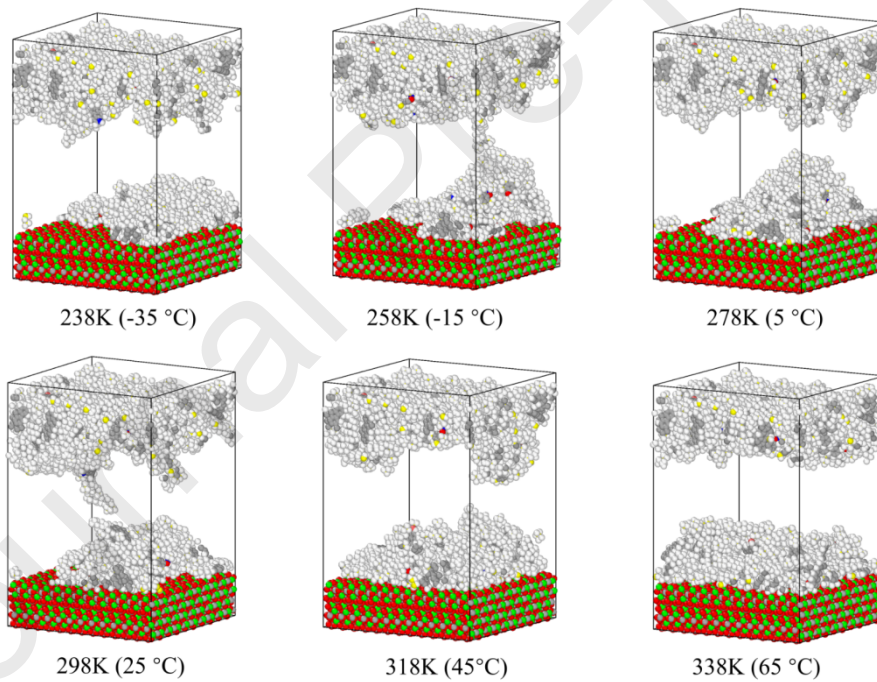
Fig. 13 Stereograms of the interfaces after pull-off debonding simulation at different temperatures

238K (-35 °C) 258K (-15 °C) 278K (5 °C)

298K (25 °C) 318K (45°C) 338K (65 °C)
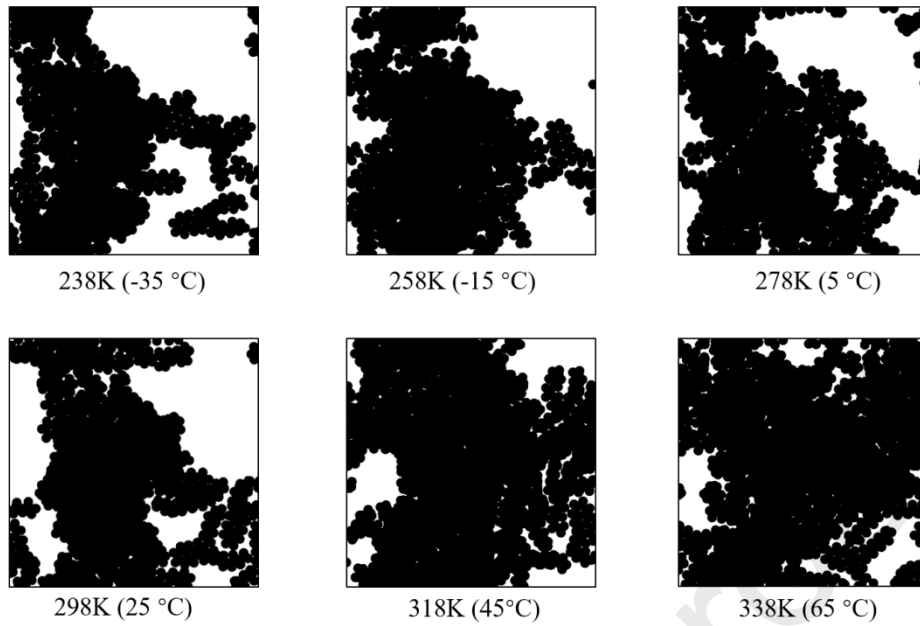
Fig. 14 Biniarized top view of residual bitumen molecules at different temperatures

Fig.14 shows that, as the temperature rises, the area covered by the residual bitumen molecules on the calcite surface becomes larger, i.e., the cohesive debonding percentage increases and the adhesive debonding percentage decreases with temperature. The percentages of the cohesive debonding were calculated for different temperature conditions, as shown in Fig. 15.
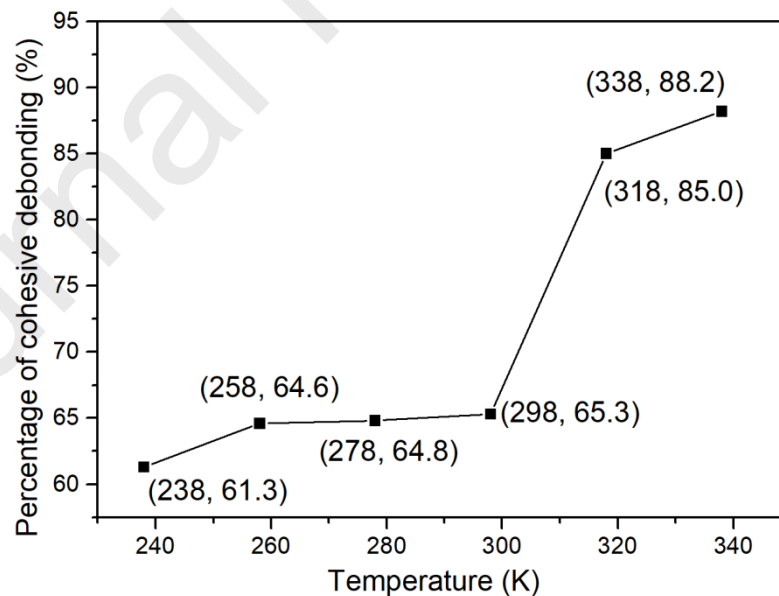
Fig. 15 Percentages of the cohesive debonding at different temperatures

As shown in Fig. 14, the percentage of cohesive debonding at interface tends to increase with temperature, from 61.3% at 238 K (-35 °C) to 88.2% at 338 K (65 °C). It is noted that when the temperature increases from 238 K (-35 °C) to 298 K (25 °C), the cohesive debonding percentage

increases from 61.3% to 65.3%, with only 4% increment. However, when the temperature exceeds 298 K (25 °C), the percentage of cohesive debonding surges, reaching 88.2% at 338 K (65 °C). This indicates that at relative low temperatures, the debonding behavior of the bitumen-aggregate interface is less sensitive to temperature and the cohesive debonding percentage remain stable, around 65%. However, when the temperature is higher than 298 K (25 °C), it has a significant effect on the debonding behavior of the interface, which shows that the cohesive debonding increasingly dominates the interfacial debonding at the high temperatures.

6.2 Interaction energy at different temperatures

The interaction energy curves during interfacial debonding at different temperatures are shown in Fig. 16. It can be seen from the figure that the interaction energies after failure show an overall increasing trend with temperature except for the change from 258K (-15 °C) to 278K (5 °C). Meanwhile, the variations in the interaction energy after debonding are insignificant in the region from 238 K (-35 °C) to 298 K (25 °C), while the interaction energy after 298 K (25 °C) shows a considerable increase. These changes explain the findings for the percentage of cohesive debonding in Fig. 15.
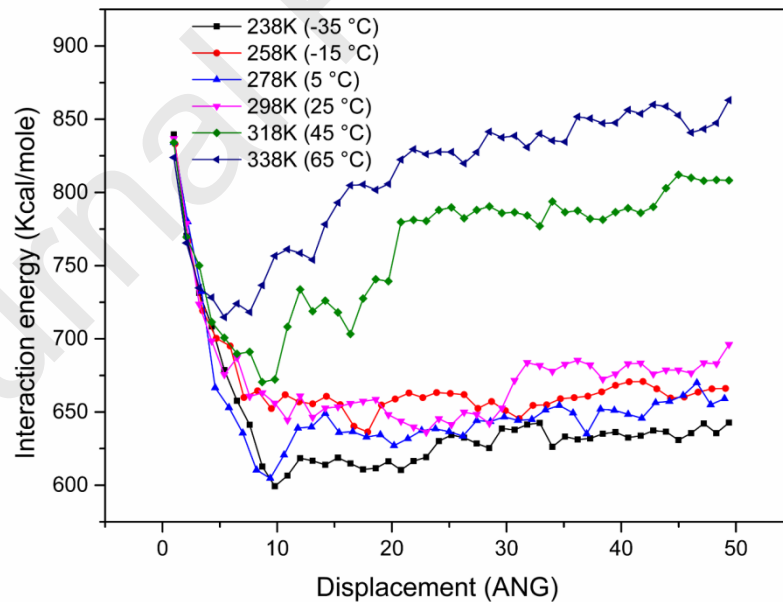
Fig. 16 Interface energy between the bitumen and the calcite aggregate at different temperatures

The higher cohesive debonding at higher temperatures is related to the motion behaviors of the bitumen molecules. As the temperature increases, the mean square displacement (MSD) of bitumen

molecules increases and their vibration amplitude increases [37]. In this case, the bituminous molecular chains are loosened and the density becomes lower, so debonding is prone to occur within the bitumen molecules when subjected to pulling forces, leading to a higher percentage of cohesive debonding .

6.3 Verification from laboratory pull-off tests on temperature effect

Wang et al. [60] conducted pull-off tests to evaluate the failure type at bitumen-aggregate interfaces. As is indicated in Table 6, the adhesive failure only appears at low temperature of 20 $°C$. As temperature rises (greater than 30°C), only cohesive debonding exists in both original bitumen and SBS modified bitumen. Note that a quantitative comparison between the experimental results and the molecular dynamic simulations was infeasible due to the scale gap. However, a similar trend that the adhesive debonding shifts to the cohesive debonding can still be identified.

Table 6 Failure type of bitumen-aggregate at different temperatures

Temperature (°C)	Original bitumen	SBS modified bitumen
20	Adhesive	Adhesive
30	Cohesive	Cohesive
40	Cohesive	Cohesive
50	Cohesive	Cohesive
55	Cohesive	Cohesive

7 Effects of mineral types on interfacial debonding behavior

7.1 Debonding behavior of bitumen-quartz aggregate interface

Fig. 17 shows the results of the bitumen-quartz interface after the pull-off simulation at different bitumen film thicknesses. It is manifest that, under the pull-off loading, the bitumen-quartz models shows adhesive debonding only which all debonding between the bitumen and quartz occurs along the interfaces when the thickness of the bitumen film ranges from 10 Å to 20 Å. The results illustrate that the adhesion ability of quartz to bitumen is weak compared with that of bitumen to calcite, which is consistent with the results obtained in laboratory tests for the adhesion ability of bitumen to different minerals [61]. This is because quartz is an electrically neutral mineral and has little electrostatic interaction with bitumen, thus the bonding between the bitumen and quartz relies

on the weak van de Waals forces [40].
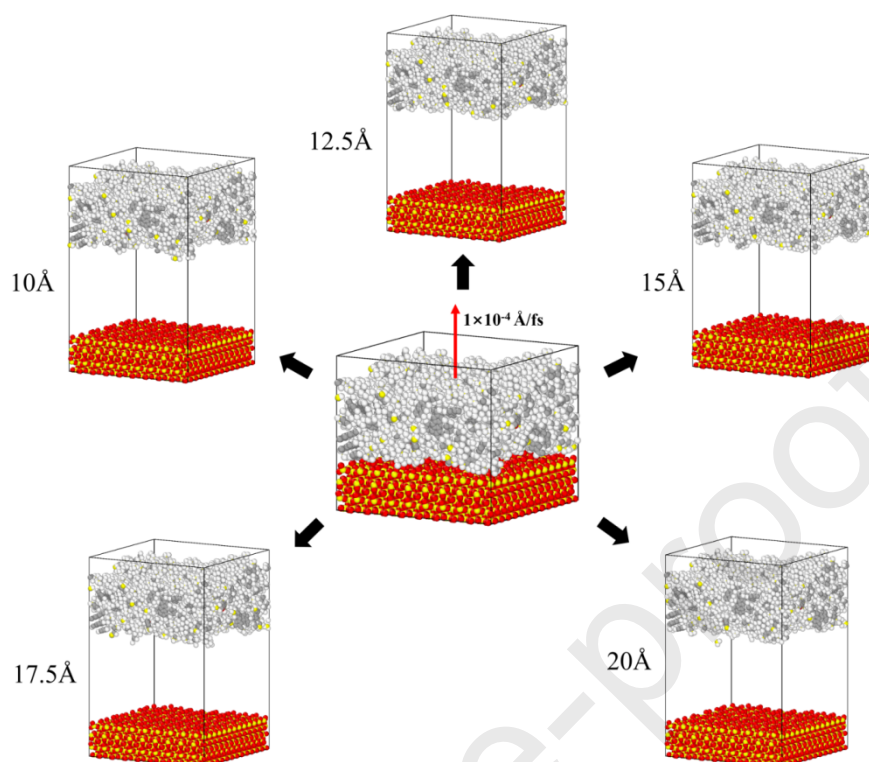
Fig. 17 Stereograms of the bitumen-quartz interface after pull-off simulation at different

bitumen thicknesses

7.2 Debonding behavior of bitumen-microcline aggregate interface

Fig. 18 shows the MD models of the bitumen-microcline aggregate interface after pulling at

different bitumen film thicknesses. It can be seen that, after pull-off simulations, the amount of

bitumen remaining on the aggregate surface, i.e., the cohesive debonding occurs. However, when

the thickness of the bitumen film is less than 20 Å, the bitumen molecules cannot completely

separate from the microcline aggregate surface after pulling, but molecular chains are formed

between the mobile bitumen and the aggregate. This indicates that in this thickness range, there is a

dynamic balance between the adhesion of the bitumen molecules to the microcline and the cohesion

within the bitumen molecules. For this reason, the fixed bitumen cannot attract all the bitumen

molecules away from the microcline surface. When the bitumen film is thin, there are always some

bitumen molecules attracted by the microcline due to its high polarity as a strong alkaline. However,

when the thickness is greater than 17.5Å, the inhomogeneous density distribution of the bitumen

molecules lead to a strong interaction between the lower part of the bitumen molecules and the

microcline aggregate and a relatively weak interaction within bitumen molecules. This results in a completely cohesive debonding within bitumen molecules.

Coulombic electrostatic interaction is dominant in the interaction between alkaline minerals (calcite and microcline) and bitumen. Compared to calcite, microcline has a stronger alkalinity with many electrostatic positive charges, so there are more electrostatic interactions between microcline and bitumen [41], which exhibits a stronger adhesion effect with bitumen, leading to an increased percentage of the cohesive debonding [62].
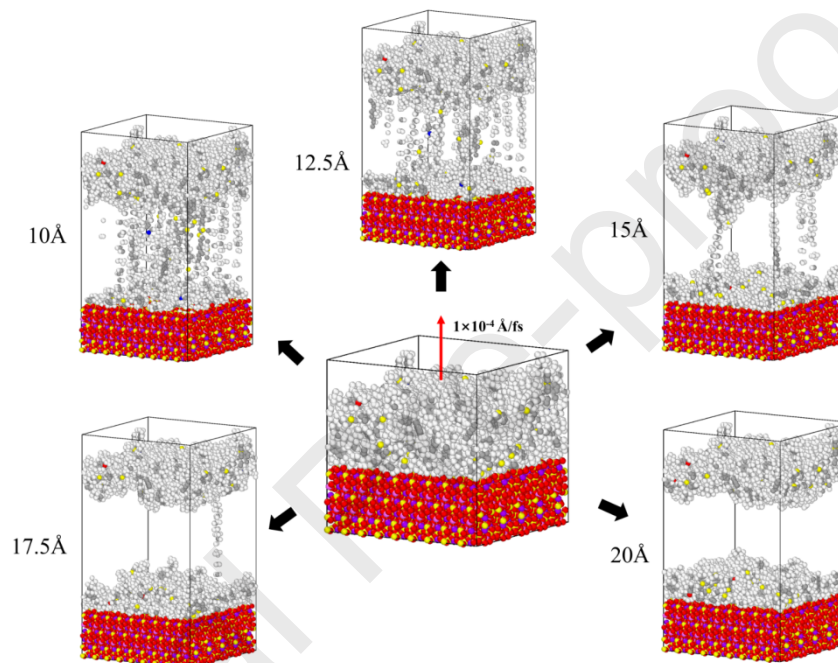
Fig. 18 Stereograms of the bitumen-microcline interface after pull-off simulation at different bitumen thicknesses

7.3 Verification from surface free energy tests on mineral type effect

Khan et al. [63] studied the adhesive properties of the interfaces between different minerals and bitumen in dry and wet conditions. The adhesive bond strength ratio below represents the adhesion properties of different minerals to bitumen. Lower ratio means the interface is insensitive to moisture and exhibits stronger adhesion to bitumen. In Table 7, it is manifest that the microcline has the strongest adhesion to bitumen and quartz has the weakest adhesion to bitumen, while calcite is in the middle. Compared to the simulation results of different mineral-bitumen models in this study, it can be found that the results are consistent.

Table 7 Ratios of adhesive bond strength in dry condition to wet condition for different

minerals

Mineral	Adhesive bond strength ratio
Calcite	5.77
Quartz	14.46
Microcline	0.88

9 Summaries and conclusions

Adhesive debonding and cohesive debonding at bitumen-aggregate interface dominate the strength and the crack resistance of the asphalt mixture. Finding out the debonding mechanism at bitumen-aggregates interfaces under different conditions will help to (a) prevent crack occurrences and improve the cracking resistance of asphalt mixtures; (b) offer a direction for selecting and modifying the raw materials in engineering. In this study, the adhesive and cohesive debonding of the bitumen-aggregate interface were investigated by performing pull-off simulations using molecular dynamics (MD). The bitumen-calcite aggregate interface was constructed to study the debonding behaviors affected by various factors, including bitumen film thickness (at 15 Å, 17.5 Å, 20 Å, 22.5 Å and 25 Å), pull-off velocity (at 5×10^{-5} Å/fs, 7.5×10^{-5} Å/fs, 1×10^{-4} Å/fs, 1.25×10^{-4} Å/fs and 1.5×10^{-4} Å/fs) and temperature [at 238K (-35 °C), 258K (-15 °C), 278K (5 °C), 298K (25 °C), 318K (45 °C)]. Moreover, quartz and microcline were also used to build interfacial models at different bitumen thicknesses to study the debonding behavior of the bitumen separated from different minerals. All the simulation results are compared with results available from the literature. The main results are displayed as follows.

(1) The bitumen-calcite aggregate interface suffers from more cohesive debonding at thicker bitumen films, increasing from 29% at 15 Å to 65% at 25 Å. There is a huge increment between 15 Å to 17.5 Å in the cohesive debonding percentage from 29% to 57%, which indicates that the debonding is more sensitive to smaller thickness. The stabilized interaction energies of the interfaces show that the adhesion strength gets stronger at a higher thickness, which is consistent with the calculated percentage of cohesive debonding. This can be explained by weak boundary layer theory

that a least cohesion region exists at a certain thickness.

(2) Pull-off velocity has a negative effect on the cohesion performance of bitumen. With an increasing pull-off velocity, the percentage of cohesive debonding presents a steady decrease, from 86% at 5×10^{-5} Å/fs to 59% at 1.5×10^{-4} Å/fs. Meanwhile, the stabilized interaction energy indicates that the adhesion of the residual bitumen becomes weaker with the increased pull-off velocity. The possible mechanism for these results is that higher pull-off velocity induces elastic molecular network in bitumen molecules, so the mobile bitumen molecules clinging to the fixed bitumen molecules are pulled off the mineral surface.

(3) Temperature can weaken the cohesion of bitumen on the calcite mineral. The percentage of the cohesive debonding grows with temperature, and especially at the range from 298K (25 °C) to 338K (65 °C), which demonstrates that the debonding is more significant at higher temperatures. The main reason for this result is that the bitumen molecules are loosened at higher temperatures and easily within the bitumen molecules.

(4) As a strong alkaline, microcline shows strong adhesion with bitumen, where all pull-off failures are cohesive debonding regardless of the bitumen film thickness. Quartz shows weak adhesion with bitumen, where pull-off failures are adhesive debonding regardless of bitumen thickness.

(5) The debonding behaviors predicted using molecular dynamics are consistent with those obtained from laboratory tests at different material, loading and environmental circumstances. These factors include bitumen film thickness, pull-off velocity, temperature and mineral types.

Future research will focus on larger-scale simulation such as coarse-grained molecular dynamics simulation to expand the dimensions of the model and achieve thicker bitumen film.

References

1. Adlinge, S.S. and A. Gupta, *Pavement deterioration and its causes.* International

Journal of Innovative Research and Development, 2013. **2**(4): p. 437-450.

2. Li, H., X. Luo, W. Yan, and Y.J.M.o.M. Zhang, *Energy-based mechanistic approach for crack growth characterization of asphalt binder.* Mechanics of Materials, 2020. **148**: p. 103462.

3. Li, H., X. Luo, and Y. Zhang, *A kinetics-based model of fatigue crack growth rate in bituminous material.* International Journal of Fatigue, 2021. **148**: p. 106185.

4. Li, L., Y. Gao, and Y. Zhang, *Crack length based healing characterisation of bitumen at different levels of cracking damage.* Journal of Cleaner Production, 2020. **258**: p. 120709.

5. Luo, X., B. Birgisson, and R.L. Lytton, *Kinetics of healing of asphalt mixtures.* Journal of Cleaner Production, 2020. **252**: p. 119790.

6. Luo, X., H. Li, Y. Deng, and Y. Zhang, *Energy-Based kinetics approach for coupled viscoplasticity and viscofracture of asphalt mixtures.* Journal of Engineering Mechanics, 2020. **146**(9): p. 04020100.

7. 361-16, A.T., *Determining Asphalt Binder Bond Strength by Means of the Binder Bond Strength (BBS) Test.* 2016, AASHTO: Washington, DC.

8. Lytton, R.L., E.A. Masad, C. Zollinger, R. Bulut, and D.N. Little, *Measurements of surface energy and its relationship to moisture damage.* 2005.

9. Zhang, Y., X. Luo, R. Luo, and R.L. Lytton, *Crack initiation in asphalt mixtures under external compressive loads.* Construction and Building Materials, 2014. **72**: p. 94-103.

10. Packham, D., *The mechanical theory of adhesion.* Handbook of Adhesive Technology, 2003: p. 69-93.

11. Packham, D. *The mechanical theory of adhesion–A seventy year perspective and its current status.* in *First International Congress on Adhesion Science and Technology.* 1998. VSP Netherland.

12. Hefer, A.W., D.N. Little, and R.L. Lytton, *A synthesis of theories and mechanisms of bitumen-aggregate adhesion including recent advances in quantifying the effects of water.* Journal of the association of asphalt paving technologists, 2005. **74**(139): p. e196.

13. Bagampadde, U., U. Isacsson, and B. Kiggundu, *Impact of bitumen and aggregate composition on stripping in bituminous mixtures.* Materials and structures, 2006. **39**(3): p. 303-315.

14. Tan, Y. and M. Guo, *Using surface free energy method to study the cohesion and adhesion of asphalt mastic.* Construction and Building Materials, 2013. **47**: p. 254-260.

15. Liu, S., X. Yu, and F. Dong, *Evaluation of moisture susceptibility of foamed warm asphalt produced by water injection using surface free energy method.* Construction and Building Materials, 2017. **131**: p. 138-145.

16. Yang, Q., S.L. Xiao, X. Qiu, X.H. Luo, and Y.J. Wang. *Mechanics mechanism analysis of asphalt-aggregate interface damage.* in *Key Engineering Materials.* 2016. Trans Tech Publ.

17. Packham, D.E., *Theories of fundamental adhesion.* Handbook of adhesion technology, 2011: p. 9-38.

18. Tarrer, A. and V. Wagh, *The effect of the physical and chemical characteristics of the aggregate on bonding.* 1991, Strategic Highway Research Program, National Research Council Washington, DC.

19.   Jamieson, I., J. Moulthrop, and D. Jones, *SHRP results on binder-aggregate adhesion and resistance to stripping.* THE ASPHALT YEARBOOK, 1995.

20.   Veytskin, Y., C. Bobko, C. Castorena, and Y.R. Kim, *Nanoindentation investigation of asphalt binder and mastic cohesion.* Construction and Building Materials, 2015. **100**: p. 163-171.

21.   Azarhoosh, A., G.H. Hamedi, and M.J. Azarhoosh, *The influence of cohesion and adhesion parameters on the moisture sensitivity of modified Asphalt mixtures with polymer additive.* The Journal of Adhesion, 2020: p. 1-23.

22.   Liu, M., S. Han, J. Pan, and W. Ren, *Study on cohesion performance of waterborne epoxy resin emulsified asphalt as interlayer materials.* Construction and Building Materials, 2018. **177**: p. 72-82.

23.   Park, D.-W., W.-J. Seo, J. Kim, and H.V. Vo, *Evaluation of moisture susceptibility of asphalt mixture using liquid anti-stripping agents.* Construction and Building Materials, 2017. **144**: p. 399-405.

24.   Hamedi, G.H. and S. Tahami, *The effect of using anti-stripping additives on moisture damage of hot mix asphalt.* International Journal of Adhesion and Adhesives, 2018. **81**: p. 90-97.

25.   Du, C., Y. Sun, J. Chen, H. Gong, X. Wei, and Z. Zhang, *Analysis of cohesive and adhesive damage initiations of asphalt pavement using a microstructure-based finite element model.* Construction and Building Materials, 2020. **261**: p. 119973.

26.   Wang, H., J. Wang, and J. Chen, *Micromechanical analysis of asphalt mixture fracture with adhesive and cohesive failure.* Engineering Fracture Mechanics, 2014. **132**: p. 104-119.

27.   ASTM. *Standard test method for pull-off strength of coatings using portable adhesion testers*. 2009. ASTM West Conshohocken, PA.

28.   Zhang, J., G.D. Airey, and J.R. Grenfell, *Experimental evaluation of cohesive and adhesive bond strength and fracture energy of bitumen-aggregate systems.* Materials and Structures, 2016. **49**(7): p. 2653-2667.

29.   Moraes, R., R. Velasquez, and H.U. Bahia, *Measuring the effect of moisture on asphalt–aggregate bond with the bitumen bond strength test.* Transportation Research Record, 2011. **2209**(1): p. 70-81.

30.   Chaturabong, P. and H.U. Bahia, *Effect of moisture on the cohesion of asphalt mastics and bonding with surface of aggregates.* Road Materials and Pavement Design, 2018. **19**(3): p. 741-753.

31.   Canestrari, F., F. Cardone, A. Graziani, F.A. Santagata, and H.U. Bahia, *Adhesive and cohesive properties of asphalt-aggregate systems subjected to moisture damage.* Road Materials and Pavement Design, 2010. **11**(sup1): p. 11-32.

32.   Yuan, Y., X. Zhu, and L. Chen, *Relationship among cohesion, adhesion, and bond strength: From multi-scale investigation of asphalt-based composites subjected to laboratory-simulated aging.* Materials and Design, 2020. **185**: p. 108272.

33.   Tang, B., Y. Ding, H. Zhu, X. Cao, *Study on Agglomeration Variation Pattern of Asphalt Molecules.* China Journal of Highway and Transport, 2013, **26**(003): p. 50-56. (in Chinese)

34.   Chen, L., Z. Zhao, H. Chen, X. Wang, and H. Xiang, *Rheological Characteristics*

and Molecular Dynamics Simulation of Interface Regeneration Between Virgin and Aged Asphalts. China Journal of Highway and Transport, 2019, **32**(03): p. 25-33. (in Chinese)

35. Zhang, L. and M.L. Greenfield, *Analyzing properties of model asphalts using molecular simulation.* Energy & fuels, 2007. **21**(3): p. 1712-1716.

36. Zhang, L. and M.L. Greenfield, *Relaxation time, diffusion, and viscosity analysis of model asphalt systems using molecular simulation.* The Journal of chemical physics, 2007. **127**(19): p. 194502.

37. Xu, G. and H. Wang, *Study of cohesion and adhesion properties of asphalt concrete with molecular dynamics simulation.* Computational Materials Science, 2016. **112**: p. 161-169.

38. Xu, G. and H. Wang, *Molecular dynamics study of oxidative aging effect on asphalt binder properties.* Fuel, 2017. **188**: p. 1-10.

39. Xu, G., H. Wang, and W. Sun, *Molecular dynamics study of rejuvenator effect on RAP binder: Diffusion behavior and molecular structure.* Construction and Building Materials, 2018. **158**: p. 1046-1054.

40. Wang, H., E. Lin, and G. Xu, *Molecular dynamics simulation of asphalt-aggregate interface adhesion strength with moisture effect.* International Journal of Pavement Engineering, 2017. **18**(5): p. 414-423.

41. Gao, Y., Y. Zhang, F. Gu, T. Xu, and H. Wang, *Impact of minerals and water on bitumen-mineral adhesion and debonding behaviours using molecular dynamics simulations.* Construction and Building Materials, 2018. **171**: p. 214-222.

42. Gao, Y., Y. Zhang, Y. Yang, J. Zhang, and F. Gu, *Molecular dynamics investigation of interfacial adhesion between oxidised bitumen and mineral surfaces.* Applied Surface Science, 2019. **479**: p. 449-462.

43. Hou, Y., L. Wang, D. Wang, X. Qu, and J. Wu, *Using a molecular dynamics simulation to investigate asphalt nano-cracking under external loading conditions.* Applied Sciences, 2017. **7**(8): p. 770.

44. Lu, Y. and L. Wang, *Atomistic modelling of moisture sensitivity: a damage mechanisms study of asphalt concrete interfaces.* Road Materials and Pavement Design, 2017. **18**(sup3): p. 200-214.

45. Lu, Y. and L. Wang, *Nanomechanics modeling of interface interactions in asphalt concrete: Traction and shearing failure study.* Journal of Multiscale Modelling, 2019. **10**(01): p. 1841004.

46. Luo, L., L. Chu, and T. Fwa, *Molecular dynamics analysis of oxidative aging effects on thermodynamic and interfacial bonding properties of asphalt mixtures.* Construction and Building Materials, 2021. **269**: p. 121299.

47. Chu, L., L. Luo, and T. Fwa, *Effects of aggregate mineral surface anisotropy on asphalt-aggregate interfacial bonding using molecular dynamics (MD) simulation.* Construction and Building Materials, 2019. **225**: p. 1-12.

48. Hill, J.-R., C.M. Freeman, and L. Subramanian, *Use of force fields in materials modeling.* Reviews in computational chemistry, 2000. **16**: p. 141-216.

49. Omairey, E.L., F. Gu, and Y. Zhang, *An equation-based multiphysics modelling framework for oxidative ageing of asphalt pavements.* Journal of Cleaner Production, 2021. **280**: p. 124401.

50. D–09, A., *Standard test method for separation of asphalt into four fractions.* 2009,

American Society for Testing Materials West Conshohocken, PA.

51. Li, D.D. and M.L. Greenfield, *Chemical compositions of improved model asphalt systems for molecular simulations.* Fuel, 2014. **115**: p. 347-356.

52. Inc., B. *Materials Studio.* 2013.

53. Zhang, J., A.K. Apeagyei, G.D. Airey, and J.R. Grenfell, *Influence of aggregate mineralogical composition on water resistance of aggregate–bitumen adhesion.* International Journal of Adhesion and Adhesives, 2015. **62**: p. 45-54.

54. Plimpton, S.J.J.o.c.p., *Fast parallel algorithms for short-range molecular dynamics.* 1995. **117**(1): p. 1-19.

55. Stukowski, A., *Visualization and analysis of atomistic simulation data with OVITO–the Open Visualization Tool.* Modelling and Simulation in Materials Science and Engineering, 2009. **18**(1): p. 015012.

56. Howson, J., E. Masad, D. Little, and E. Kassem, *Relationship between bond energy and total work of fracture for asphalt binder-aggregate systems.* Road Materials and Pavement Design, 2012. **13**(sup1): p. 281-303.

57. Boiziau, C. and G. Lecayon, *Adhesion of polymers to metals: A review of the results obtained studying a model system.* Surface Interface Analysis, 1988. **12**(9): p. 475-485.

58. Howson, J.E., *Relationship between surface free energy and total work of fracture of asphalt binder and asphalt binder-aggregate interfaces.* Vol. 73. 2011.

59. Gent, A., *Adhesion of viscoelastic materials to rigid substrates. II. Tensile strength of adhesive joints.* Journal of Polymer Science Part A-2: Polymer Physics, 1971. **9**(2): p. 283-294.

60. Wang, X., J. Ren, X. Gu, N. Li, Z. Tian, and H. Chen, *Investigation of the adhesive and cohesive properties of asphalt, mastic, and mortar in porous asphalt mixtures.* Construction and Building Materials, 2021. **276**: p. 122255.

61. Lyne, Å.L., P. Redelius, M. Collin, and B. Birgisson, *Characterization of stripping properties of stone material in asphalt.* Materials and structures, 2013. **46**(1): p. 47-61.

62. Mirzababaei, P., *Effect of zycotherm on moisture susceptibility of Warm Mix Asphalt mixtures prepared with different aggregate types and gradations.* Construction and Building Materials, 2016. **116**: p. 403-412.

63. Khan, A., P. Redelius, and N. Kringos, *Evaluation of adhesive properties of mineral-bitumen interfaces in cold asphalt mixtures.* Construction and Building Materials, 2016. **125**: p. 1005-1021.

Author Statement

Pengxu Chen: Investigation, Formal analysis, Data curation, Methodology, Software, Writing - original draft

Xue Luo: Project administration, Resources, Supervison

Yangming Gao: Software, Validation

Yuqing Zhang: Conceptualization, Data curation, Methodology, Resources, Supervision, Writing - review & editing.
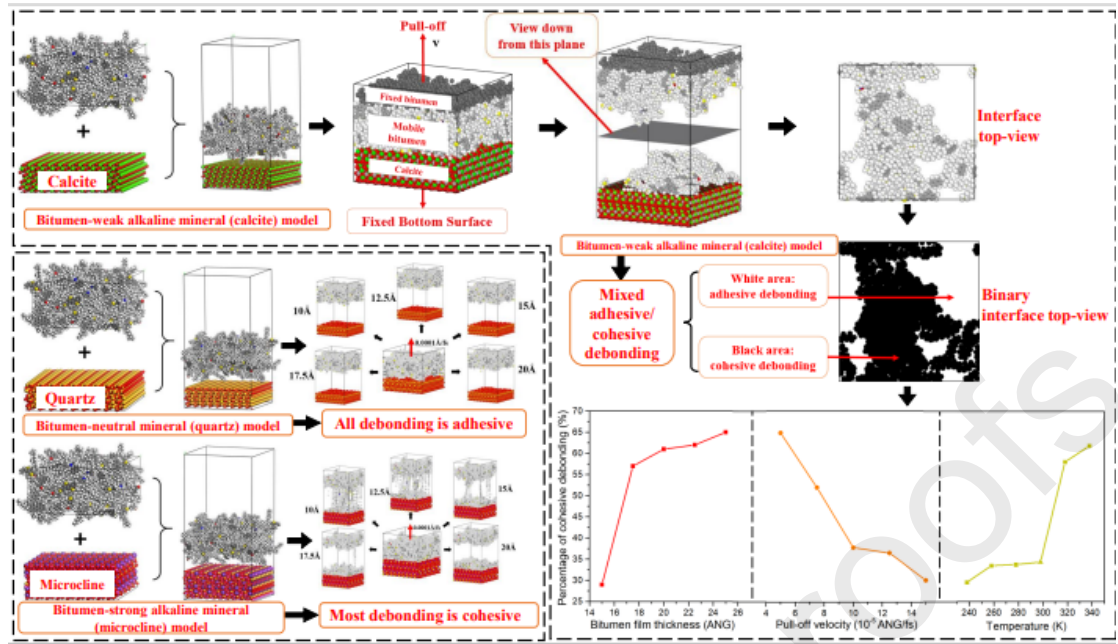
Highlights

Paper "Modelling percentages of cohesive and adhesive debonding in bitumen-aggregate interfaces using molecular dynamics approaches"

- Molecular pull-off simulation of bitumen-aggregate interface was performed.
- Cohesive debonding percentage rises with bitumen film thickness and temperature.
- Less cohesive and more adhesive debonding occur at higher pull-off velocities.
- Stronger alkaline minerals are more prone to have cohesive debonding.

Declaration of interests

☒ The authors declare that they have no known competing financial interests or personal relationships that could have appeared to influence the work reported in this paper.

☐The authors declare the following financial interests/personal relationships which may be considered as potential competing interests: